Transient liquid phase Ag-based solder technology for high-temperature packaging applications

Sharif, Ahmed; Gan, Chee Lip; Chen, Zhong

2013

Transient Liquid Phase Ag-based Solder Technology for High-temperature Packaging Applications

Ahmed Sharif[1], Chee Lip Gan[2], Zhong Chen[2]

1. Department of Materials & Metallurgical Engineering, Bangladesh University of Engineering and Technology, Dhaka 1000, Bangladesh

2. School of Materials Science & Engineering, Nanyang Technological University, Singapore 639798

Corresponding Author: Dr. Ahmed Sharif, Tel: (+88)-01912802486, Fax: (+88)-029665618,
E-mail: "Dr. Ahmed Sharif" asharif@mme.buet.ac.bd

Abstracts

A lead-free Ag-based soldering technique through transient-liquid-phase (TLP) bonding is proposed in this study for high-temperature microelectronic packaging applications. The solder paste, which contained Ag and Sn powders with a no-clean flux, was used to join Cu substrates. The setup was bonded at 250°C for 10 minutes. The study focuses on mechanical and microstructural characterizations of the joints. The shear strength measured at 250°C shows good high temperature performance of the joint. The effects of Ag and Sn contents on mechanical, electrical and thermal properties of sintered bulk Ag-Sn samples were also investigated independently. The results demonstrate that the Ag-Sn TLP bonding is an effective interconnection method for harsh environment electronic packaging.

Key words: Harsh environment; microelectronics packaging; transient-liquid-phase; high-temperature reliability; intermetallic compounds.

Introduction

Harsh environment electronics calls for devices that are capable of surviving extreme environment conditions such as high ambient temperature, high pressure and others [1]. High-lead (Pb) solders such as Pb-5Sn and Pb-10Sn (mass%) alloys with melting points of 310°C and 305°C, respectively, are presently granted immunity from the Restriction of Hazardous Substances (RoHS) requirements for their use in electronic systems operating in high temperature and pressure, especially in military, geophysical logging and space applications [2, 3]. The efforts to find Pb-free replacements for the high temperature applications have achieved very limited success so far [4]. One of the key reasons is that the reliability of the solder is directly linked to its operating temperature. For instance, the melting point of a solder should be more than 443°C to operate at 300°C (i.e. 0.8 times of the melting point of the alloy). Furthermore, current candidate solders like Ag-alloys, Zn-alloys, and Au–based alloys have many limitations including high processing temperature, poor processability, poor corrosion resistance and high costs [5-7]. Nano-Ag has been listed in recent literature as a leading candidate for lead-free low temperature interconnect-materials [8, 9]. The commercialization of nano-Ag as solder material faces the challenges of toxicity, escalating silver price and availability of industrial bonding equipment [9]. Transient liquid phase (TLP) bonding has been widely used in the joining of different types of materials [10-1516]. The process engages different low melting point materials between the base metals to be joined and relies on interactions for isothermal solidification at the bonding temperature. The integrity of the resulting joints is enriched by the presence of the liquid phase during bonding, yet the bonds are able to withstand operation at temperatures above the bonding temperature once solidification is complete [1617].

2

The aim of this work is to evaluate lead-free Ag-Sn solder paste through transient liquid phase (TLP) bonding as a solder material for high temperature applications. The study focuses on mechanical and microstructural characterizations of the joint on Cu substrates with different compositions of Ag and Sn content.

Experimental procedure

In this study, silver (Ag) and tin (Sn) powders with average particle sizes of < 5 μm were used for the base matrix materials. Initially Ag and Sn powders were mixed thoroughly to prepare samples for the properties characterization of bulk materials. The resulting powder mixtures were uniaxially pressed to form pallets. The resulting pallets were pressurelessly sintered in air at 250°C for 10 minutes. A Nabertherm (model: N 7/H, Germany) resistance heating box furnace was used to perform the sintering process. The furnace was calibrated with a tolerance of less than ± 3°C. The Vickers hardness test was performed on the sintered pallets in air using a (SHIMADZU HSV-20) microhardness tester. The electrical resistance measurements were carried out using the four-point probe method with a Keithley 2400 to source the current and a HP 34401A for the voltage measurements.

The thermal stability of the sintered pallets was measured by differential scanning calorimeter (DSC Q 10). The temperature range was scanned from 25°C to 1000°C at a rate of 20 K/min under nitrogen gas atmosphere.

Consequently, both Ag and Sn powders were mixed with a no clean flux to prepare a paste and then applied in between two 5 mm-thick Cu substrates as shown in Fig.1. Ag-Sn solder paste bonding consists of two main steps: screen printing and sintering. Using a stainless steel stencil, the paste was dispensed on the 5 mm X 5 mm Cu substrates and then 2.5 mm X 2.5 mm Cu

substrates were placed on them. Then the pasted Cu-to-Cu substrates were sintered at 250°C for 10 minutes under a bonding pressure of 1.2 MPa to complete the joining process.

Shear test was performed on bonded samples by using a Dage Series 4000 Bond Tester. Shear tool height of 100 µm and shear speed of 100µm/s were applied during the test. Shear strength measurements were carried out at both ambient and 250°C to evaluate room and high temperature performance. For the high temperature shear measurement, the sample stage was heated to 250°C and each sample was left on the sample stage for 15 minutes to reach the equilibrium temperature before the test was carried out. A total of 20 Cu/Cu joints were shear tested for each condition.

The joined samples were mounted in an epoxy mold before being ground and polished for SEM examination. The microstructural analysis was carried out using a Philips XL 40 FEG (Philips Electron Optics, The Netherlands) scanning electron microscope (SEM). For the compositional analysis, energy dispersive X-ray analysis (EDAX International, Mahwah, NJ) was performed in the SEM.

Results and discussions

Fig. 2 shows the microhardness and the electrical resistivity measurement of the bulk Ag-Sn samples of different compositions respectively. It is found that the microhardness increased with the Ag content up to 75wt. % then decreased again. The microhardness of the bulk $Ag_{75}Sn_{25}$ (i.e. 75 wt. % Ag and 25 wt. % Sn) system showed the highest value. Electrical resistivity of the bulk sample showed a decreasing trend with the addition of Ag (Fig. 2). As anticipated the 100 wt. %

4

Ag containing sample showed the lowest resistivity. Most importantly with the formation of 100% Ag_3Sn IMCs in the $Ag_{75}Sn_{25}$ system, the resistivity did not show any significant change.

Fig. 3 shows the DSC curves of the three different Ag-Sn systems. From the DSC curves, it is found that for $Ag_{70}Sn_{30}$ (i.e. 70 wt. % Ag and 30 wt. % Sn), some Sn still remained unreacted. From the Ag-Sn phase diagram, it can be seen that Ag_3Sn formation stoichiometrically requires 73.17% wt. of Ag and 26.83 wt.% of Sn (Fig. 4) [1718]. Above 26.8 wt.% of Sn in the matrix, there should be some Sn left unreacted which would deteriorate the high temperature mechanical strength of the structure. As predicted, no unreacted Sn was observed with 75% Ag, on the other hand some unreacted Ag was noticed in both the heating and cooling curves of $Ag_{75}Sn_{25}$. For high temperature operation it is expected that no Sn should be remained in the bulk to maintain its mechanical integrity. Under such requirement, Sn in the Ag-Sn TLP system should be around 25 wt. % or less. The melting point of Ag_3Sn intermetallic compound (IMC) is around 480°C (Fig. 4) and it is expected that if the Ag-Sn mixture converts to Ag_3Sn IMC after reaction at 250°C, it will survive high temperature operations at 250°C and above. From bulk material analysis, it seems that the high Ag containing (75 wt. % and above) Ag-Sn solder would be the better choice for joining.

Form Fig. 5 4 it is noticed that the shear strength increased with Ag content initially and then decreased. $Ag_{60}Sn_{40}$ solder showed the highest shear strength. Beyond that, the shear strength measured at the room temperature and high temperature (i.e. 250°C) showed a decreasing trend. An important finding is that the high temperature strength level of low Ag containing Ag-Sn joints with Cu substrates maintained comparable level with room temperature shear. Beyond 70wt.% of Ag, a significant drop was observed in the high temperature shear strength as

5

compared to the room temperature shear. With the prescribed bonding technology, the 100wt.% Ag containing solder joint showed the lowest shear strength.

With 50 wt. % and 60 wt. % of Ag the shear strength of the joints ranged between 24 MPa to 32 MPa (Fig. 54). The sintering at 250°C for 10 minutes ensured that all the Sn consumed by the IMC forming reactions either with Ag particles or the Cu substrates. Thus even with 50 wt. % of Sn the shear strength measured at high temperature did not show any significant reduction. The shear results at high temperature confirmed that there was no Sn left in the $Ag_{50}Sn_{50}$ joint. In this case the excess Sn after Ag_3Sn formation (i.e. 50-26.83=23.17 wt.%) reacted with Cu substrates to form Cu-Sn IMCs at the interfaces.

These results demonstrate that Cu/Ag–Sn/Cu joints with 40-50 wt. % Sn has greater solder joint integrity as compared to that with higher of amount of Ag. To investigate the shear load and the reaction of the solder joints, a detailed cross-sectional study was carried out by revealing the cross-sectional microstructures. Fig. 65 shows the optical micrographs of the Cu to Cu bonded structures with the Ag-based solders. It was found that the thickness of the joint varied between 25-40 µm for all the cases. The variation in thickness of the Ag-based joint was due to manual screen printing method. Fig. 76 shows the SEM figures of the interfaces of the Cu substrates with the Ag-Sn solders. Bonding using the different amount of Ag and Sn containing solder proceeded under the same conditions. Significant differences were revealed between the interfaces and sintered bulk solder layers arising from using the high Ag containing (70 wt. % and above) Ag-Sn solder than that from using the sintered high Sn (40-50 wt. %) containing Ag-Sn solder. The joint using the sintered high Sn (40-50 wt. %) containing Ag-Sn solder had a denser sintered solder layer than the joint using the high Ag containing (70 wt. % and above) Ag-Sn solder (Fig. 65 and 76). Another thing is that the interfacial layer was also thicker for the

6

high Sn containing Ag-based solder than that for the high Ag containing Ag-based solder (Fig. 76).

During sintering at 250°C, when Sn particles melted, the liquid phase wetted the Ag particles and causes shrinking of the whole solder volume by eliminating the pores inside the bulk solder. With high amount of Sn, the amount of liquid phase formation was also high and consequently the sintered solder layer became denser through liquid phase sintering. In addition, Sn wetted the Cu layer to form a thick interfacial Cu-Sn IMC layers. For up to 60 wt. % Ag containing solders, thick layers of Cu_6Sn_5 and Cu_3Sn IMCs were observed at the interfaces using backscattered electron micrograph (Fig. 7a6a). It is suggested that the molten Sn reacted with the surrounding Ag initially and then the excessive Sn reacted with the Cu substrates and formed Cu_6Sn_5 during bonding at 250°C. Once the Sn was fully reacted, Cu_3Sn compounds were formed at the interface as a result of conversion of Cu_6Sn_5 under Cu-rich condition. This suggests that the high amount of Sn significantly improved the bondability to Cu.

In the case of the joint using the high Ag containing (70 wt. % and above) Ag-Sn solder, there were voids observed at the Ag/Cu interface (Fig. 7b6b). With fewer amounts Sn in the solder, the amount of liquid Sn could be even insufficient for Ag reaction. Hence, the solid state sintering was dominant mechanism for bonding the high Ag containing Ag-Sn aggregate. It is already well known that solid state sintering is slower than the liquid state sintering process. Solid state sintering require high amount of pressure and time for denser structure. As a result, the bulk sintered solder had high amount of porosity in the microstructure (Fig. 7b6b). Consequently there will be insufficient Sn to react with Cu substrate in this case. Thus the interface was devoid of Cu-Sn IMCs. The joint shear strength of both room temperature and high temperature of the high Ag containing (i.e. 70 wt. % and above) solder ranged between 2 MPa to 19 MPa (Fig. 54).

7

After measuring the shear loads, fractured surfaces of the residue Cu pads and sheared Ag-Sn joints were immediately studied by optical microscope and SEM. The typical fracture surfaces on the bottom Cu substrates are shown in Fig. 87. In general, there were two main failure modes observed after the shearing tests. The first type of fracture occurred at a location near but lower than the shearing height (100 μm), leaving a thick layer of solder on the Cu pad (Fig. 8a7a). The EDX analysis along the fracture surface of the $Ag_{60}Sn_{40}$ solder revealed Ag-Sn compound (Fig. 8a7a). In this case, the fracture propagated through the bulk Ag-Sn solder. This indicates that the solder/pad interfacial Cu-Sn IMCs was much stronger than the shear strength of the bulk Ag_3Sn IMC. It is worth mentioning that that the average modulus of the Ag_3Sn IMC was 86 GPa, which was considerable lower than that of Cu-Sn IMCs (i.e. above 100GPa) [1819].

For 70% and above Ag containing solder, the fracture propagates along the joint interface (Fig. 8b 7b and 8c7c). EDX analysis revealed that the silver grey layer observed on the bottom Cu substrate surface consisted of Ag-Sn IMC for $Ag_{75}Sn_{25}$ solder (Fig. 8b7b). While on the radish reddish region of the pad surface as shown in Fig. 8b 7b only Cu was found. In this case, Ag and Sn reacted to form Ag_3Sn compound in the bulk as the amount of Ag and Sn was very close to the stoichiometry (i.e. 73.17 wt. % Ag and 26.83 wt. % Sn) for Ag_3Sn compound formation. Therefore it is understandable that Ag-Sn reaction takes place much faster in the bulk than Cu-Sn at the interface. As a result, the interface was the weakest link in the joint (Fig. 54). It is also important to report that the solubility of Sn in Ag at 250°C is around 9 wt.%.

For joint using 100% Ag, EDX analysis revealed that the radish silver layer on the bottom Cu pad side consisted of Ag and Cu (Fig. 8c7c). EDX results on the brown region of the pad showed only Ag (Fig. 8c7c). Although the interface at the Cu/Ag system was established by the diffusional bonding through mutual interchange of the Cu and Ag atoms, the interfacial bonding

8

was still very weak (Fig. ~~5~~4). As a result, the strength level of high Ag containing solder showed a substantial decrease at high temperature than that at room temperature. It is expected that higher sintering temperature along with high pressure would be needed for better interfacial strength with high Ag containing solder.

Conclusions

From bulk material analysis, it was thought that the high Ag containing (75 wt. % and above) Ag-Sn solder would be the better choice for joining. Later on, it was established that a higher amount of Sn content than the stoichiometric ratio needed for the formation of Ag_3Sn compound was better for joining Cu under bump metallurgy with the prescribed bonding technology. The Cu-to-Cu joint made using the Ag-Sn TLP bonding had a denser interfacial microstructure between the Cu substrates and the sintered low Ag (50-60 wt.%) containing Ag-based solder than that using the high Ag containing (70 wt.% and above) Ag-based solder. Reflecting the difference in the bonding mechanism, the joint shear strength of the low Ag containing solder was 22–35 MPa, which was significantly higher than that of the high Ag-containing solder of 2.0–19 MPa. Most importantly, the joints of the Cu/ low-Ag containing Ag-Sn solder/Cu systems maintained their integrity even when shear-tested at 250°C. The fracture position of the Cu-to-Cu joint with the high Sn containing Ag-Sn solder was predominantly in the bulk Ag-Sn solder, while that with the high Ag-containing Ag-Sn solder was at the interface between the Cu substrate and the sintered Ag layer.

References

1. Y. C. Liu, J. W. R. Teo, S. K. Tung, K. H. Lam. High-temperature creep and hardness of eutectic 80Au/20Sn solder. J. Alloys Compd. 448 (2008) 340-343.

2. C. P., Lin, C. M. Chen, Y. W. Yen, H. J. Wu, S. W. Chen. Interfacial reactions between high-Pb solders and Ag. J. Alloys Compd. 509 (2011) 3509-3514.

3. S. W. Park, T. Sugahara, K. S. Kim, K. Suganuma. Enhanced ductility and oxidation resistance of Zn through the addition of minor elements for use in wide-gap semiconductor die-bonding materials. J. Alloys Compd. 542 (2012) 236–240.

4. A. Sharif, J. Z. Lim, R. I. Made, F. L. Lau, E. J. R. Phua, J. D. Lim, C. C. Wong, C. L. Gan, Z. Chen. Pb-Free Glass Paste: A Metallization- Free Die-Attachment Solution for High- Temperature Application on Ceramic Substrates. J. Electron. Mater. 42 (2013) 2667-2676.

5. V. Chidambaram, J. Hald, J. Hattel. Development of Au–Ge based candidate alloys as an alternative to high-lead content solders. J. Alloys Compd. 490 (2010) 170-179.

6. N. Kang, H. S. Na, S. J. Kim, C. Y. Kang. Alloy design of Zn–Al–Cu solder for ultra high temperatures. J. Alloys Compd. 467 (2009) 246-250.

7. K. Suganuma, S. Sakamoto, N. Kagami, D. Wakuda, K. S. Kim, M. Nogi. Low-temperature low-pressure die attach with hybrid silver particle paste. Microelectron. Reliab. 2012; 52: 375-380.

8. T. Wang, X. Chen, G. Q. Lu, G. Y. Lei. Low-temperature sintering with nano-silver paste in die-attached interconnection. J. Electron. Mater. 36 (2007) 1333-1340.

9. K. S. Siow. Mechanical properties of nano-silver joints as die attach materials. J. Alloy Compd. 2012; 514: 6-19.

10. M. Pouranvari, A. Ekrami, A. H. Kokabi. Solidification and solid state phenomena during TLP bonding of IN718 superalloy using Ni-Si-B ternary filler alloy. J. Alloys Compd. 563 (2013) 143-149.

11. M. Pouranvari, A. Ekrami, A. H. Kokabi. Microstructure development during transient liquid phase bonding of GTD-111 nickel-based superalloy. J. Alloys Compd. 461 (2008) 641-647.

12. N. P. Wikstrom, A. T. Egbewande, O. A. Ojo. High temperature diffusion induced liquid phase joining of a heat resistant alloy. J. Alloys Compd. 460 (2008) 379-385.

13. X. Y. Gu, D. Q. Sun, L. Liu, Z. Z. Duan. Microstructure and mechanical properties of transient liquid phase bonded TiC_P/AZ91D joints using copper interlayer. J. Alloys Compd. 476 (2009) 492-499.

14. J. D. Liu, T. Jin, W. Li, X. F. Sun, H. R. Guan, Z. Q. Hu. Creep fracture mechanism of TLP joint of a Ni-base single crystal superalloy. J. Alloys Compd. 457 (2008) 185-190.

15. J. Wang, K. Li, H. Li, W. Li, Z. Li, L. Guo. Partial transient liquid phase bonding of carbon/carbon composites using $Ti-Ni-Al_2O_3-Si$ compound as interlayer. J. Alloys Compd. 550 (2013) 57-62.

16. J.F. Li, P.A. Agyakwa, and C.M. Johnson, Kinetics of Ag3Sn growth in Ag-Sn-Ag system during transient liquid phase soldering process, Acta Mater. 2010; 58: 3429-3443.

16.17.   N.S. Bosco, F.W. Zok, Critical interlayer thickness for transient liquid phase bonding in the Cu–Sn system, Acta Mater. 2004; 52: 2965-2972.

17.18.   I. Karakaya, W.T. Thompson, The Ag-Sn (silver-tin) system, Bull. Alloy Phase Diagrams 1987; 8: 340-347.

18.19.   J. P. Lucas, H. Rhee, F. Guo, K. N. Subramanian. Mechanical properties of intermetallic compounds associated with Pb-free solder joints using nanoindentation. J. Electron. Mater. 32 (2003) 1375-1383.

List of Figures

Fig. 1 Schematic drawing of the bonding arrangement (not to scale)

Fig. 2 Variation of microhardness and electrical resistivity of bulk solder for different proportion of Ag.

Fig. 3 DSC curves of $Ag_{70}Sn_{30}$, $Ag_{75}Sn_{25}$ and $Ag_{80}Sn_{20}$ solder alloys on both heating and cooling.
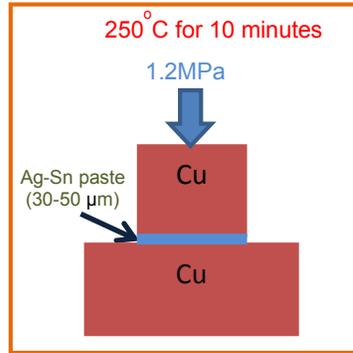
~~Fig.4 Silver-Tin phase diagram [17].~~

Fig. ~~5~~ 4 Shear strength of the solder joints with different Ag compositions in Ag-Sn solder alloys.

Fig. ~~6~~ 5 Optical micrographs showing the bonded structures after joining with (a) $Ag_{50}Sn_{50}$ and (b) $Ag_{100}Sn_0$.

Fig. ~~7~~ 6 SEM micrographs showing the interfaces after joining Cu with (a) $Ag_{60}Sn_{40}$ and (b) $Ag_{70}Sn_{30}$ solder alloys.

Fig. ~~8~~ 7 Bottom Cu substrate side fracture surfaces with (a) $Ag_{60}Sn_{40}$, (b) $Ag_{75}Sn_{25}$ and (c) Ag_{100} solder alloys.
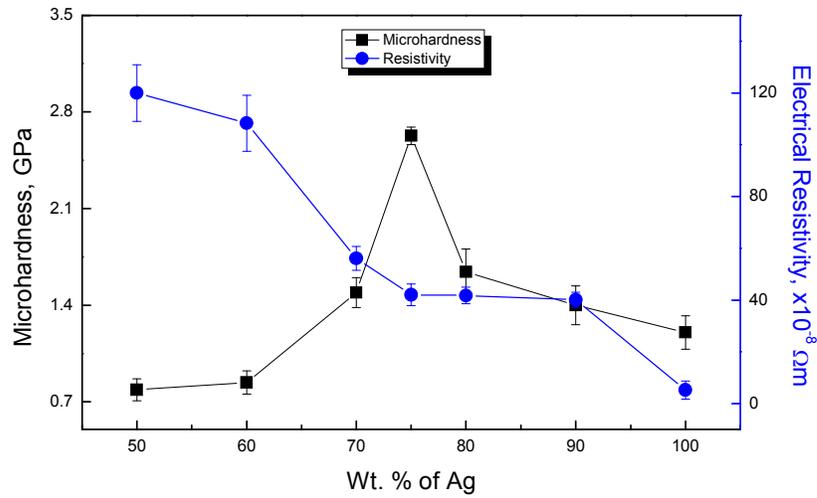
Fig. 1 Variation of microhardness and electrical resistivity of bulk solder for different proportion of Ag.
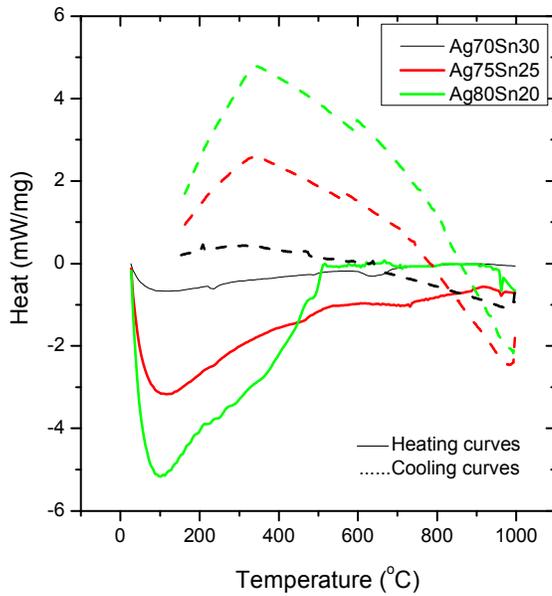
Fig. 2 DSC curves of $Ag_{70}Sn_{30}$, $Ag_{75}Sn_{25}$ and $Ag_{80}Sn_{20}$ solder alloys on both heating and cooling.

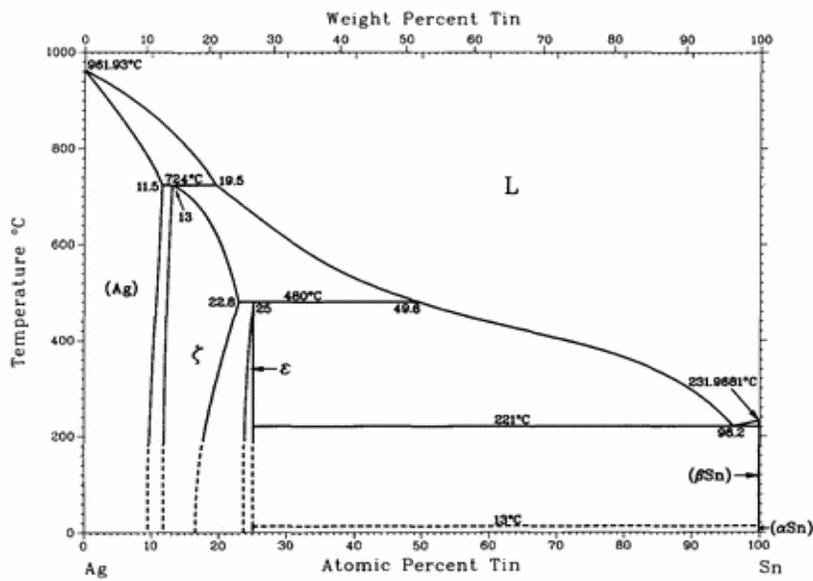Fig. 3 Schematic drawing of the bonding arrangement (not to scale)

Fig.4 Silver-Tin phase diagram [17].

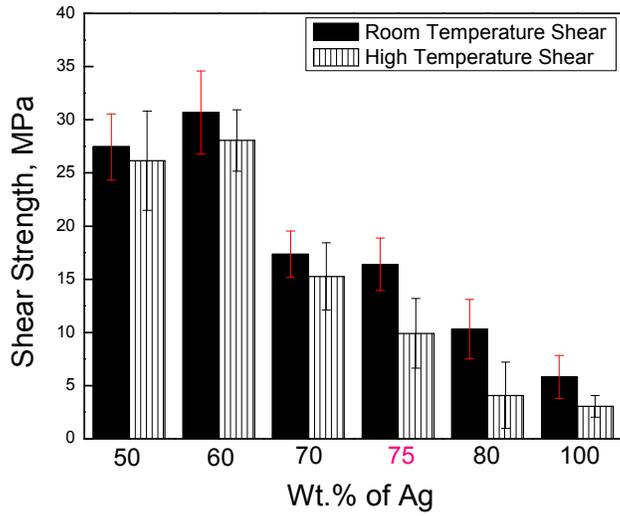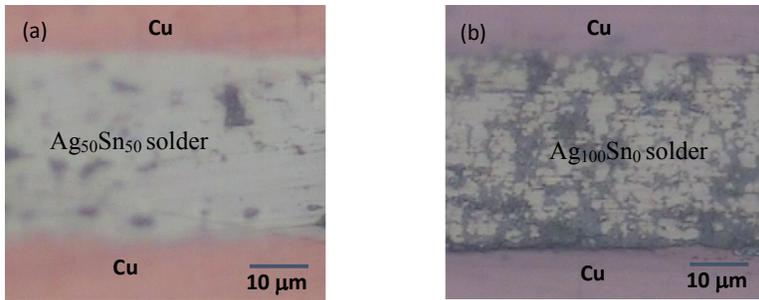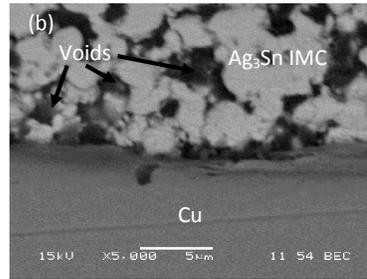Fig. 5 4 Shear strength of the solder joints with different Ag compositions in Ag-Sn solder.

Fig. 6 5 Optical micrographs showing the Cu to Cu bonded structures after joining with (a) $Ag_{50}Sn_{50}$ and (b) $Ag_{100}Sn_0$.
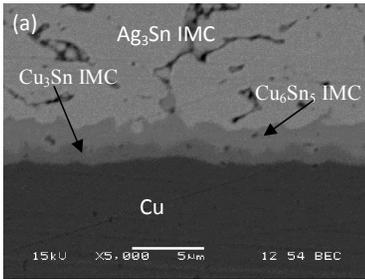
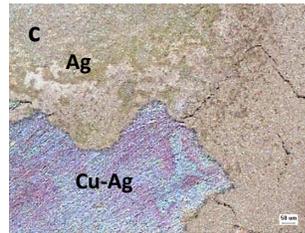Fig. 7 6 SEM micrographs showing the interfaces after joining on Cu with (a) $Ag_{60}Sn_{40}$ and (b) $Ag_{70}Sn_{30}$

Fig. 8 7 Bottom Cu substrate side fracture surfaces with (a) $Ag_{60}Sn_{40}$, (b) $Ag_{75}Sn_{25}$ and (c) Ag_{100}.